Normality in State Uncertainties from Orbit Determination results fitting Optical Measurements

Sven K. Flegel
Space Environement Research Centre (SERC) Ltd.
Weston Creek, ACT 2611, Australia

James Bennett
Electro Optic Systems Pty Ltd.
Queanbeyan, NSW 2620, Australia

ABSTRACT

Two fundamentally different approaches to determine normality of state uncertainty are compared by application to a range of test cases. The first method is the Henze-Zirkler test, which operates on a random particle sample. The variability of its result is quantified. Using this method, breakdown of state normality has been found to occur in three stages which are detailed. The second test compares the offset of the sample from the unscented transform to the mean of the covariance in whitened space. This test is much more efficient than the random particle based approach and can be applied using any perturbations model. The comparison is performed on the state uncertainty in Cartesian space and using two-body motion without process noise. The more efficient, unscented transform based approach shows promising results in first comparisons.

1 INTRODUCTION

The state uncertainty of space objects is utilised in a variety of applications including collision probability estimation, manoeuvre detection, track association, multi-target tracking and sensor scheduling. Each of these areas has its own accuracy and realism requirements of the uncertainty. As traditional orbit determination methods produce a state fit to observations based on root-mean-square minimisation, the state uncertainty at and for a time after epoch is Gaussian. Methods building on this information therefore typically rely on this distribution. However, over time normality breaks down, impacting the applicability of these methods. The aim of the current work is to perform an automatic assessment of the timeframe until breakdown of Gaussianity of the state uncertainty of all orbit determination results, which are introduced into the catalogue being set up by the Space Environment Research Centre (SERC Limited). Supplying this information as meta-data will help users chose appropriate methods when working with the state uncertainty supplied through the catalogue.
In the current paper, two fundamentally different approaches are outlined to determine normality of state uncertainty. The first method is the Henze-Zirkler test, which belongs

to the family of consistent approaches and operates on a random particle sample. As the test result varies based on the given sample, rigorous assessment requires Monte-Carlo based analyses. Furthermore, non-linearities in the relative motion of particles increase with distance. This creates a dependence of the test results at predicted epochs on the compactness of the initial sample, which translates into sample size. The final test result is based on a hypothesis test for which the confidence level is set to the commonly accepted value of 95%. As the method does not rely on any other assumptions, it is applied here as a baseline for comparison. The second test relies solely on the unscented transform. The offset of the sample mean to that of the obtained covariance matrix in whitened space is used to test for normality. The comparatively small sample size makes this approach efficient. It does however contain a tuneable decision threshold parameter, which is calibrated here by comparing the two methods based on their results for a select number of test cases. The comparison is performed on the state uncertainty in cartesian space. For the calibration, state and uncertainty predictions rely on two-body motion and assume no process noise. In the comparison, an emphasis is put on the time after epoch at which non-Gaussianity is first detected. The paper concludes by applying both approaches to a select number of orbit determination results from SERC's catalogue.

2 MULTIVARIATE NORMALITY TEST BASELINE

The random sample approach was chosen to create a baseline for the assessment of the breakdown of normality in state uncertainty predictions. At least in theory it relies on fewer assumptions than more efficient tests such as the ones described in [2, 3]. It does however suffer from two major drawbacks: 1) Different tests for multivariate normality (MVN) will give different results in particular when samples are 'near' normally distributed. 2) The outcome depends to some quantifiable degree on the sample drawn. The latter issue can be overcome by calculating the result based on a large number of samples, which in turn can be computationally expensive. The former requires a good understanding of available statistical tests. The following section starts out with an outline of tests presented in literature from which a suitable test is selected.

2.1 Random Sample MVN Test

[1] Results from large scale comparisons of different MVN tests which operate on random samples are published for instance in [10] and [4]. [10] split MVN tests into four categories:

- Graphical and correlational approaches
- Skewness and kurtosis approaches
- Goodness-of-fit approaches, and
- Consistent approaches.

[1] Parts of this description have been taken with only minor alterations from [5].

The well known Kolmogorov-Smirnov, Cramér-von Mises, and Anderson-Darling test all fall into the category for "Goodness-of-fit approach". Among the selected methods was an extension of the Anderson-Darling test published by [12] which is given the name Romeu–Ozturk test. The Henze–Zirkler [6] test falls into the category of "Consistent approaches". *Consistent* is used to indicate that it has been mathematically shown that the test will – at least in theory – consistently reject *all* non-MVN distributions. An example of tests of the category "Skewness and kurtosis approaches" are approaches based on the work of [9]. Among the criteria which the authors used to assess the tests was the rate of Type I[2] and Type II[3] errors as well as feasibility for implementation and desirable mathematical properties. The two major conclusions of this analysis were: a) No single test for MVN delivered perfect results and it was recommended to employ multiple methods for testing of MVN where possible; and, b) If only one test is used, the Henze–Zirkler was recommended. The Romeu–Ozturk was rejected early on in the study due to high Type I type error rates which in some cases exceeded 10 %. These results are supported by a later study by [4]. In these publications, particle sample sizes were varied between 25 and 250 and sample space dimensions of up to 10 were considered. Based on these results, the Henze–Zirkler test was selected as baseline method.

2.2 Henze-Zirkler Test for Normality

The following equation calculates the test metric:

$$HZ = \left[\frac{1}{n}\sum_{i=1}^{n}\sum_{j=1}^{n} e^{-\frac{\beta^2}{2}D_{ij}}\right] - \left[2\left(1+\beta^2\right)^{-\frac{d}{2}}\sum_{i=1}^{n} e^{-\frac{\beta^2}{2(1+\beta^2)}D_i}\right] + \left[n\left(1+2\beta^2\right)^{-\frac{d}{2}}\right] \tag{1}$$

Herein D_i is the squared Mahalanobis distance of the i^{th} observation to the centroid and D_{ij} gives the Mahalanobis distance between i^{th} and j^{th} observations. The authors give a relation for β which uses the particle sample size n_p and sample space dimensions d:

$$\beta = \frac{1}{\sqrt{2}}\left(\frac{n(2d+1)}{4}\right)^{\frac{1}{d+4}}. \tag{2}$$

This value is used to test for the null-hypothesis H_0 which is that the sample is indeed MVN distributed. In general, the test statistic HZ is small when the particles are MVN distributed and increases with deviation from MVN. For a complete description of its implementation, the reader is referred to [5].

2.2.1 Example Evolution of Henze-Zirkler MVN Test Values

[4] Using the fast Mikkola/Halley-4 single step solution for two-body motion as detailed in [11], a common structure is observed in all simulations performed to date of which an

[2]Type I error: An MVN distributed sample is incorrectly identified as being non-MVN distributed.

[3]Type II error: A non-MVN distributed sample is mistakenly identified as being MVN distributed.

[4]This description is also given in the companion-paper by James C.S. Bennett et al. "Progress in a new conjunction and threat warning service for Space Situational Awareness"

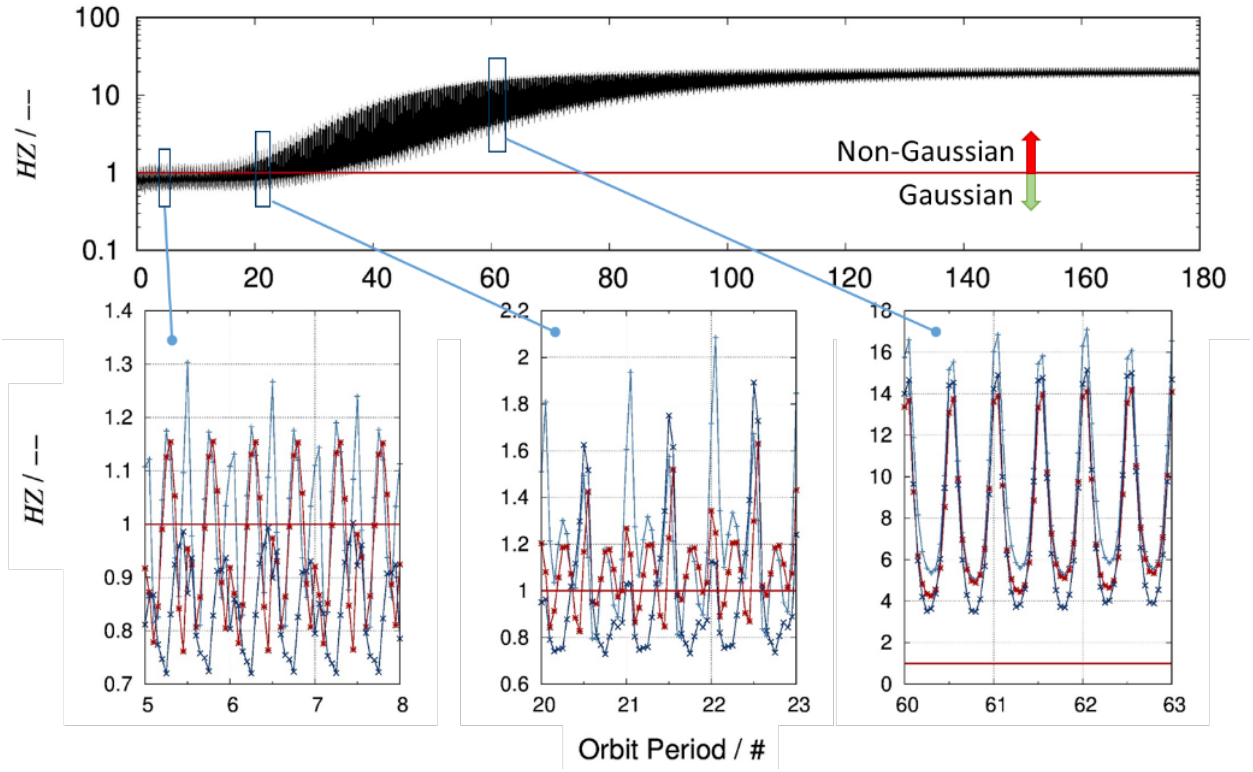

Figure 1: Example evolution of Henze-Zirkler test for multivariate normality (HZ). Three random samples were drawn from position & velocity covariance. Test is performed on position uncertainty only.

example is given in Fig. 1. In all simulations performed to date, the evolution could be split roughly into three stages: i) Fully Gaussian, ii) Partially Gaussian iii) Fully Non-Gaussian. During the initial phase following the state epoch, the uncertainty remains Gaussian throughout the entire orbit. During this stage, type I error causes some samples to still flag non-Gaussianity. The uncertainty volume then becomes non-Gaussian during parts of the orbit. During this phase, a common structure materialises between the time-evolution of all initial samples until, in the final phase, all samples exhibit the same time evolution and the uncertainty volume is non-Gaussian throughout the entire orbit. Generally, the six dimensional position & velocity uncertainty space has been found to be better behaved than the three dimensional position-only uncertainty. Furthermore, the position uncertainty has a strong half-orbit periodicity while the position+velocity uncertainty exhibits a full orbit periodicity. Finally it is observed that the position & velocity uncertainty remains Gaussian for a much shorter time than the position uncertainty.

2.2.2 Sample Size

Fig. 2 visualises the importance of proper sample size selection taken from [5]. It has been produced by predicting an object's position using only uncertainty in two dimensions of the position in ECI coordinates. The blue lines are made up of individual

particles created at the σ-lines 1 to 10 at the initial epoch where Gaussianity is given by definition. The red lines are made up of the same particles after propagation to $t_1 = t_0 + \Delta t$. To ease comparison of the two samples, the particle positions are transformed into Mahalanobis space. Within this space, particle distances from the mean are given in multiples of standard deviations. At t_1, it can be seen that while Gaussianity close to the state mean is still intact, this is not the case at 10 σ. Although the technical significance of distances at 10 σ are questionable, the same relation can be observed on any scale. To define a suitable sample size, a relation is first required between the sample size n_p and the number of particles outside a defined confidence interval p:

$$n_p\,(\nu > \nu_0) = n_p\,(1 - p(\nu_0, k = 1)) \tag{3}$$

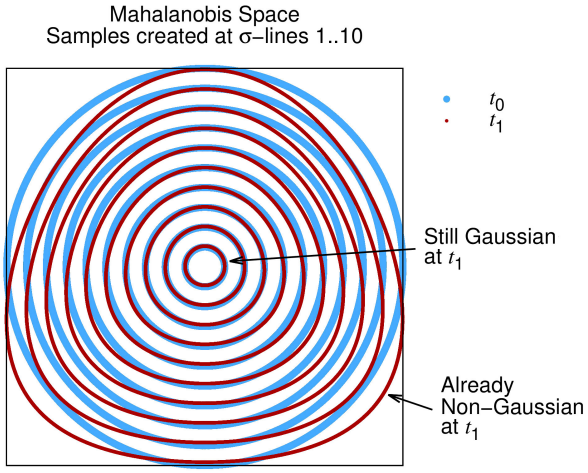

Figure 2: Particles taken at the 1-σ to 10-σ lines before propagation (t_0) and after propagation (t_1). Close to the uncertainty mean, Gaussianity is still intact after propagation while it is no longer given at 10-σ.[5]

The p-value is the area under the integrated $\chi^2(\nu, k)$ function with degrees of freedom k that is *outside* the defined limit variance ν_0. For $k = 1$, the χ^2 function describes the distribution of residuals of the one-dimensional normal distribution. For the current purpose, the 3-σ bound (99.7 % confidence level) is selected as the limit beyond which no significant particles are required. In addition, a *significant* number of particles should still be present between $98.7\,\% \leq p \leq 99.7\,\%$ confidence levels. The 'significant number of particles is set to 30'. From Tab. 1 it can be seen that any sample size between 3 000 and 11 000 satisfies the above restrictions. With the understanding visualised in Fig. 2, larger sample sizes lead to earlier detection of non-MVN. For the current purpose it is decided to ere on the conservative side and a sample size of $n_p = 10{,}000$ is chosen. This is the same number as was selected in previous studies.

Table 1: Sample sizes and the number of particles in the outskirts of the distribution.

	Confidence Level	
Sample Size	98.7 % – 99.7 %	> 99.7 %
500	5.0	1.3
1 000	10.0	2.7
2 000	20.0	5.4
3 000	30.0	8.1
4 000	40.0	10.8
5 000	50.0	13.5
6 000	60.0	16.2
7 000	70.0	18.9
8 000	80.0	21.6
9 000	90.0	24.3
10 000	100.0	27.0
11000	110.0	29.7

2.2.3 Monte-Carlo Runs & Central Limit Theorem

It is in the nature of the approach that for any given epoch, not all samples lead to the same MVN-test result. Often, a decision is based on the mean of all outcomes. If the Monte-Carlo simulation is repeated with different initial samples, the mean value will differ from the previous simulation, leading to a different epoch for the onset of the breakdown of normality. This variation decreases by increasing the number of Monte-Carlo runs, at a computational cost. The distribution of means from many such Monte-Carlo simulations are normally distributed, regardless of the distribution of outcomes from individual samples. The standard deviation of the distribution of mean values $\sigma_{\bar{x}}$ between such 'batches' of Monte-Carlo runs can then be estimated from the standard deviation of a single sample s and the number of Monte-Carlo simulations n_{mc} used to obtain it:

$$\sigma_{\bar{x}}(n_{mc}) = \frac{s(n_{mc})}{\sqrt{n_{mc}}} \tag{4}$$

Finding MVN Breakdown Onset and Conclusion Epochs Once MVN starts breaking down, it initially occurs only briefly during an orbit either at one or several locations. Section 2.2.1 has details on this. To identify the state of the uncertainty at any epoch, one must therefore evaluate the entire orbit. Here, orbits are evaluated at equidistant epochs where the first and last evaluation is exactly one orbit apart. Initially, the first orbit after epoch is evaluated. Following, an orbit several days after epoch is evaluated. The results from this evaluation is then used to determine in which direction to continue the search. Breakdown onset and conclusion epochs are thus iterated towards. For the transition onset, the epoch is recorded which marks the start of the first orbit during which the MVN test has failed at least once. In the two-body propagation this is easy to do as the

orbit period remains constant. The breakdown conclusion epoch marks the start of the first orbit during which the MVN test fails at all epochs. Evaluating for MVN at set epochs allows sharp peaks to be missed. Here, circular orbits are tested at nine epochs and eccentric orbits at 17 epochs due to their increased dynamic behaviour. Using 17 epochs on a circular orbit case yielded no change in the results. Nine epochs on the high eccentric orbits however resulted in the relevant peaks to be missed and yielding markedly different results.

Breakdown evolution function The Central Limit Theorem (CLT) can now be employed to estimate the variability of the transition onset and conclusion epochs. To achieve this, first, the highest and lowest mean and standard deviation values from all runs are identified. Continuous functions which are monotonically increasing within the range of interest are then fit to the mean and standard deviations independently. An example of this is shown in Fig. 3 and 4. Values near the MVN decision threshold are given high weights in the fit. This ensures that the variability in the breakdown epoch is reflected well.

Estimating variability in MVN Breakdown epoch With $\bar{x}$ as the sample mean and $\sigma_{\bar{x}}(n_{mc})$ as the CLT standard deviation of the mean, a parameter r is introduced which, when multiplied on the known CLT standard deviation can be used to obtain the confidence level at which the MVN-Breakdown occurs for a given epoch t:

$$0 = \bar{x}(t) + r(t) \cdot \sigma_{\bar{x}}(n_{mc})(t) - 1 \tag{5}$$

t is finally solved for by fixing $r(t)$ to a predefined value R. With $R = 0$, the relation simplifies back to $0 = \bar{x}(t) - 1$ and the breakdown epoch as per the mean function fit is obtained. This relates to the 50 % confidence level $(1 - \alpha)$. Confidence level values according to the cumulative standard normal distribution are:

R	-3	-2	-1	0	1	2	3
$1-\alpha$ [%]	0.1	2.3	15.9	50.0	84.1	97.7	99.9

2.3 Baseline Scenarios

The assessment of collision probability methods performed by Alfano [1] contains detailed information on states and uncertainties for twelve different close encounter cases. These cases create the basis for the current study. Tab. 2 gives an overview of the simulated scenarios. For complete details, the reader is referred to the original publication. The first number in each case ID is the case number. The second number references the respective object from the close conjunction case. Cases number 3, 11 and 12 differ from other cases only in parameters not pertaining to the state and covariance and are thus neglected here. Instead the GEO cases have been duplicated but multiplied by a factor of 100 (IDs ending on 'a'). Case 9 has been omitted here but is very similar to Case 10.

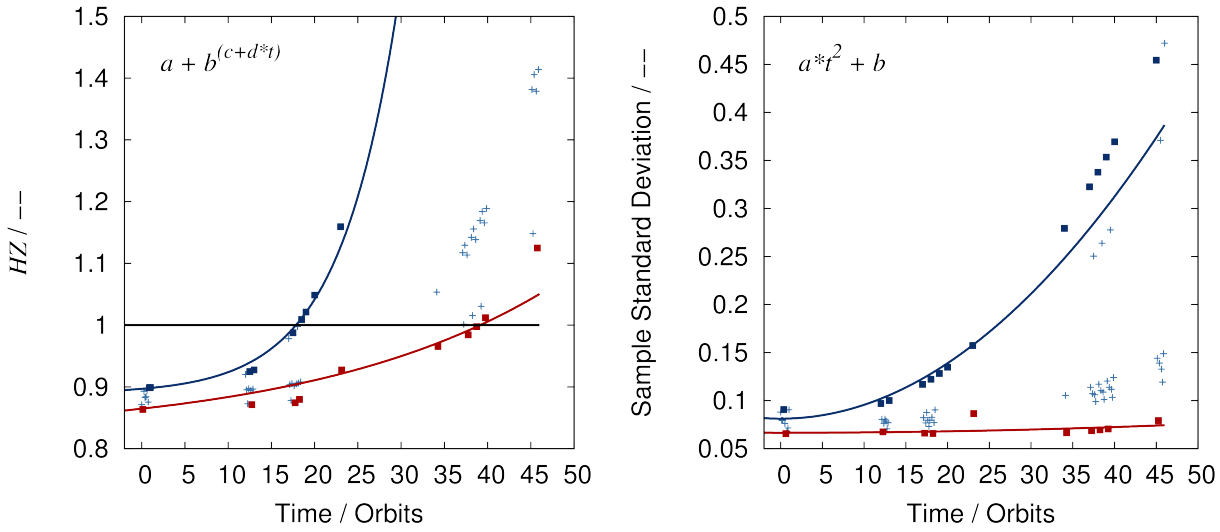

Figure 3: Simulation results from two-body propagation for Alfano's case 6-1 (see Tab. 2). Mean values from 25 Monte-Carlo runs evaluated at up to nine equidistant epochs within an orbit. *Left:* Fits to mean values for transition start (blue line) and conclusion (red line). *Right:* Fits to standard deviation values for transition start (blue line) and conclusion (red line). Light blue crosses are results at epochs which don't yield orbit minimum or maximum MVN values.

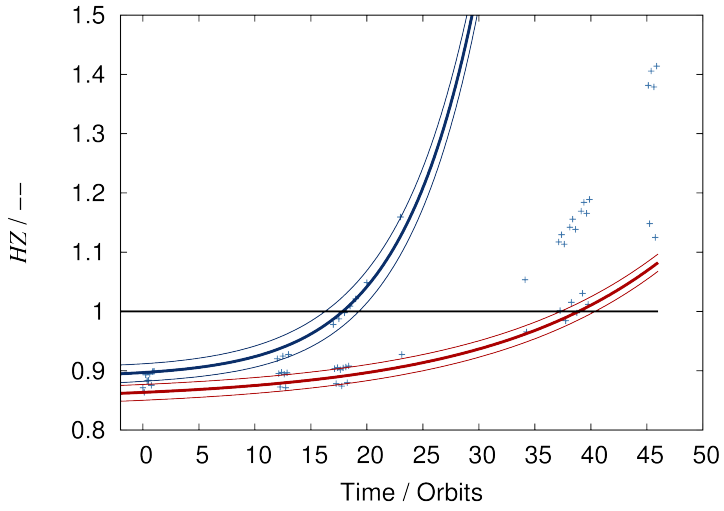

Figure 4: Results for mean and CLT standard deviation as per relation (4) and depicted in Fig. 3 superimposed.

Results for the transition onset and conclusion epochs based on the Henze-Zirkler Method and using 25 Monte-Carlo runs at a sample size of 10,000 are given in Tab. 3 and visualised in Fig. 5. The results are characterised in terms of the mean value of each Monte-Carlo analysis and its variability based on the CLT applying the method outlined in Section 2.2.3. The variability of results using the CLT is determined for the 15.9 % and 84.1 % ($\pm 1\,\sigma$) confidence levels. They are visualised in percent of estimated time interval

Table 2: Overview of calibration cases based on [1]. Nomenclature is *scenario No.-object No.*.

Case ID	1-1	3-1	4-1	1-1a	3-1a	4-1a	5-1	6-1	7-1	8-1	10-1
	1-2	3-2	4-2	1-2a	3-2a	4-2a	5-2	6-2	7-2	8-2	10-2
Orbit Type	**GEO**						**LEO**			**MEO**	**HEO**

until MVN breakdown in Fig. 6. Simply enlarging the uncertainty causes the breakdown of normality to advance in time. Although this seems correct intuitively, one should bear in mind that not all terms impact the uncertainty growth equally. For instance, an appropriate selection of covariance terms for instance have been observed to allow normality to break down later, even though variances may be higher in position as well as velocity.

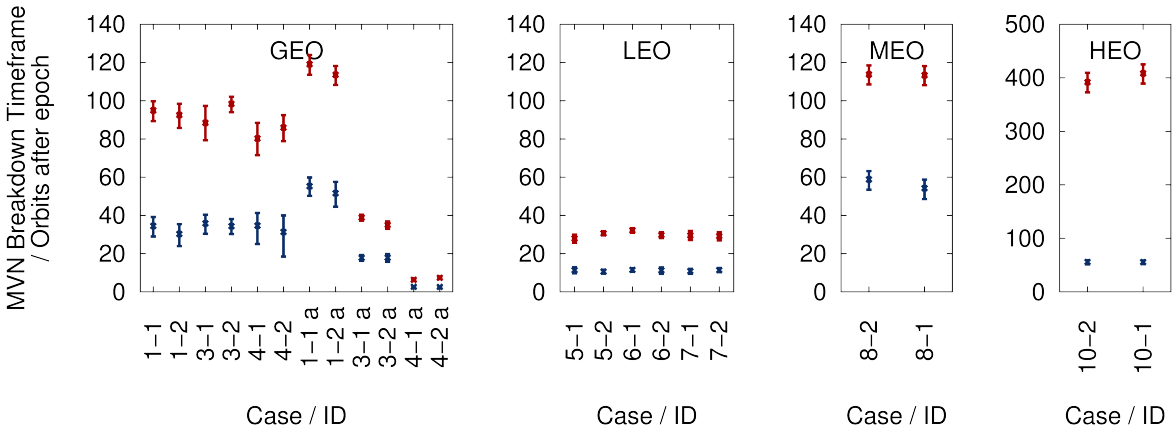

Figure 5: Beginning and end of transition into non-Gaussianity of position uncertainty. Scenario identifier refer to those detailed in Tab. 2. Errorbars are for the CLT standard deviation $\pm 1\,\sigma_{\bar{x}}$. Blue is for MVN breakdown onset epoch. Red is for MVN breakdown conclusion epoch.

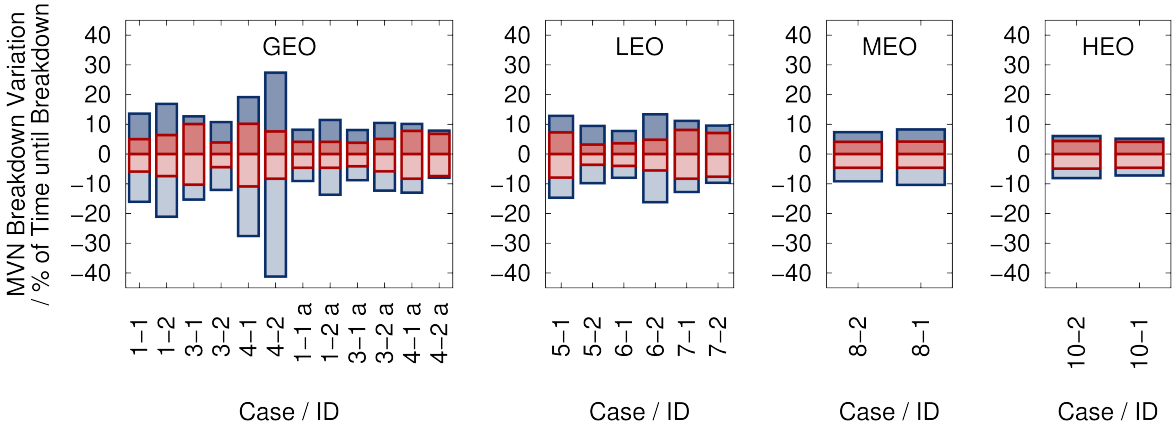

Figure 6: Variability of results in percent of the estimated time interval until MVN breakdown is detected at the Monte-Carlo mean value. Blue is for MVN breakdown onset epoch. Red is for MVN breakdown conclusion epoch.

Table 3: Beginning and end of transition into non-Gaussianity of position uncertainty. Scenario identifier refer to those detailed in Tab. 2. >days< and >orbits< refer to time after state epoch.

Id	Orbit Period	Transition starts			Transition ends		
		Mean		$+\sigma_{\bar{x}}$ / $-\sigma_{\bar{x}}$	Mean		$+\sigma_{\bar{x}}$ / $-\sigma_{\bar{x}}$
	[min]	[days]	[orbits]	[%]	[days]	[orbits]	[%]
Geosynchronous Orbits							
1-1	1396.3	34.9	36	-16.1/ 13.6	92.1	95	-5.9/ 5.0
1-2	1396.3	30.1	31	-21.1/ 16.9	89.2	92	-7.4/ 6.4
3-1	1396.3	34.9	36	-15.3/ 12.7	86.3	89	-10.3/ 10.1
3-2	1396.3	33.0	34	-12.1/ 10.8	96.0	99	-4.4/ 3.9
4-1	1396.3	34.9	36	-27.6/ 19.2	78.5	81	-10.9/ 10.2
4-2	1396.3	34.9	36	-41.2/ 27.4	82.4	85	-8.3/ 7.6
Geosynchronous Orbits, Larger Uncertainties							
1-1a	1396.3	9.7	10	-14.7/ 12.9	28.1	29	-7.9/ 7.3
1-2a	1396.3	9.7	10	-9.8/ 9.5	29.1	30	-3.6/ 3.2
3-1a	1396.3	11.6	12	-8.0/ 7.8	31.0	32	-4.0/ 3.6
3-2a	1396.3	9.7	10	-16.2/ 13.4	29.1	30	-5.5/ 4.8
4-1a	1396.3	9.7	10	-12.8/ 11.2	31.0	32	-8.3/ 8.1
4-2a	1396.3	11.6	12	-9.7/ 9.6	28.1	29	-7.6/ 7.1
Low Earth Orbits							
5-1	94.6	3.7	56	-9.1/ 8.2	7.8	118	-4.6/ 4.1
5-2	94.6	3.4	52	-13.7/ 11.5	7.4	113	-4.6/ 4.1
6-1	94.6	1.2	19	-8.8/ 8.1	2.5	38	-4.1/ 3.8
6-2	94.6	1.2	19	-12.3/ 10.5	2.3	35	-5.8/ 5.1
7-1	94.6	0.1	2	-13.0/ 10.2	0.4	6	-8.3/ 7.8
7-2	94.6	0.1	2	-8.0/ 7.9	0.5	8	-7.4/ 6.8
Medium Earth Orbits, Near Circular							
8-1	675.6	26.7	57	-9.2/ 7.4	53.0	113	-4.6/ 4.1
8-2	675.6	25.8	55	-10.4/ 8.3	53.0	113	-4.6/ 4.2
Medium Earth Orbits, Highly Eccentric							
10-1	717.7	28.4	57	-8.1/6.1	198.9	399	-4.9 / 4.4
10-2	717.7	27.4	55	-7.2/5.2	203.8	409	-4.6/ 4.1

3 EFFICIENT MVN TESTING

The transition start and end epochs described in Section 2.2.1 have different implications for different methods of covariance propagation. An error-state transition matrix approach uses a prior covariance matrix to produce an update. As no information on non-normally distributed uncertainties is contained in this representation, any covariance matrix produced after the transition phase is entered is no longer reliable. The covariance matrix propagation based on the unscented transform on the other hand allows each particle to move independently through time and space. The covariance matrix generated from these at any epoch requires no prior and so will accurately portrait normally distributed uncertainties within the transition region. The key here is to identify at each epoch, whether the underlying uncertainty space is normally distributed or not.

3.1 Unscented Transform Based MVN Test

The basic idea is that the breakdown of normality will cause the sample mean to drift from the actual covariance mean. Some normalisation however is required to decouple the drift from orbit regime and covariance size. As the random sample method is computationally very expensive, the unscented transform described by [7, 8] is used to generate independent states from the initial covariance. These are propagated through time, independently of one another. The covariance can be generated at any epoch from the particles. Here, the mean state is added with weighting of 0.6. This factor places the sigma-points roughly at the boundary of the chosen $3\,\sigma$ bound to be assessed. It's effect on the method sensitivity has not be assessed. The covariance is then used to perform a whitening transformation of the states via Cholesky Decomposition. This step is also part of the Henze-Zirkler MVN test but on a random sample and is detailed in [5]. This step normalises a normally distributed sample so that it follows the standard normal distribution in all dimensions. This step directly yields the normalised distance of the mean state from the centre of the covariance matrix.
This method is applied to the cases described in Section 2.3. The normalised distance is then extracted from the results for the $\pm 1\,\sigma_{\bar{x}}$ time window for the onset and conclusion of the breakdown of Gaussianity from Tab. 2. The results are visualised in Fig. 7. Both onset and conclusion of the breakdown of normality show consistent values given the used error bounds with the exception of Cases 1-2 and 4-2 for the onset. No overarching dependence on the covariance size or orbit altitude is observed.
Fig. 8 exemplifies the evolution of this normalised distance over time for four select cases. Generally, the evolution is very similar to that of the Henze-Zirkler Test statistic (compare Fig. 1). Between most cases, the evolution is very well behaved. Cases 1-2 and 2-4 both yielded 'outlier' results and exhibit almost identical behaviour. Only Case 1-2 is shown here. The cause is at the time of writing not understood and must be investigated further. For the well-behaved cases it can be seen that within an orbit, the test value will oscillate, depending on whether or not the distribution at that point in time is normally distributed or not. A closeup for Case 1-1 visualises this common evolution.

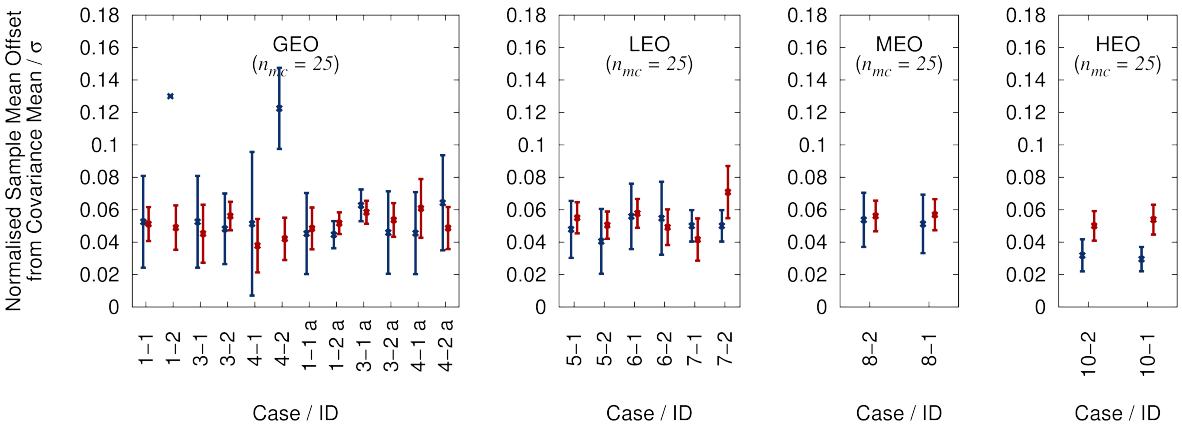

Figure 7: Position offset of sample mean from the position covariance.

4 BREAKDOWN OF NORMALITY FOR CATALOGUE OD RESULTS

Measurements from passive and active optical measurements of objects in all Earth orbits are being processed in a Batch-Least-Squares orbit determination and ingested into a catalogue. An account of the status of this catalogue is made in the companion paper "Automating the assessment of orbit predictions and estimations for building and maintaining a new catalogue" by Dr. Michael Lachut et al. as well as "Progress in a new conjunction and threat warning service for Space Situational Awareness" by Dr. James C.S. Bennett et al.. The OD results assessed here are from mid 2018 and include passive only observations.
The current section should be seen as a proof of concept as the SERC catalogue is still in its build-up phase and the presented efficient method for MVN testing is still in its early testing stage.

4.1 Overview of Cases

An overview of example orbit determination results which are assessed in the following is given in Tab. 4.

Table 4: Overview of orbit determination example cases

Orbit	GEO		LEO	MEO	HEO	
OD ID	3715 3721	3778 3783	3769 3753	3732 3739	3073	3062
NORAD	27399	36287	17973	19751	38625	34198
Name	JCSAT 8	BEIDOU G1	COSMOS 1844	ETALON 1	BREEZE-M DEB	ARIANE 42P+ DEB

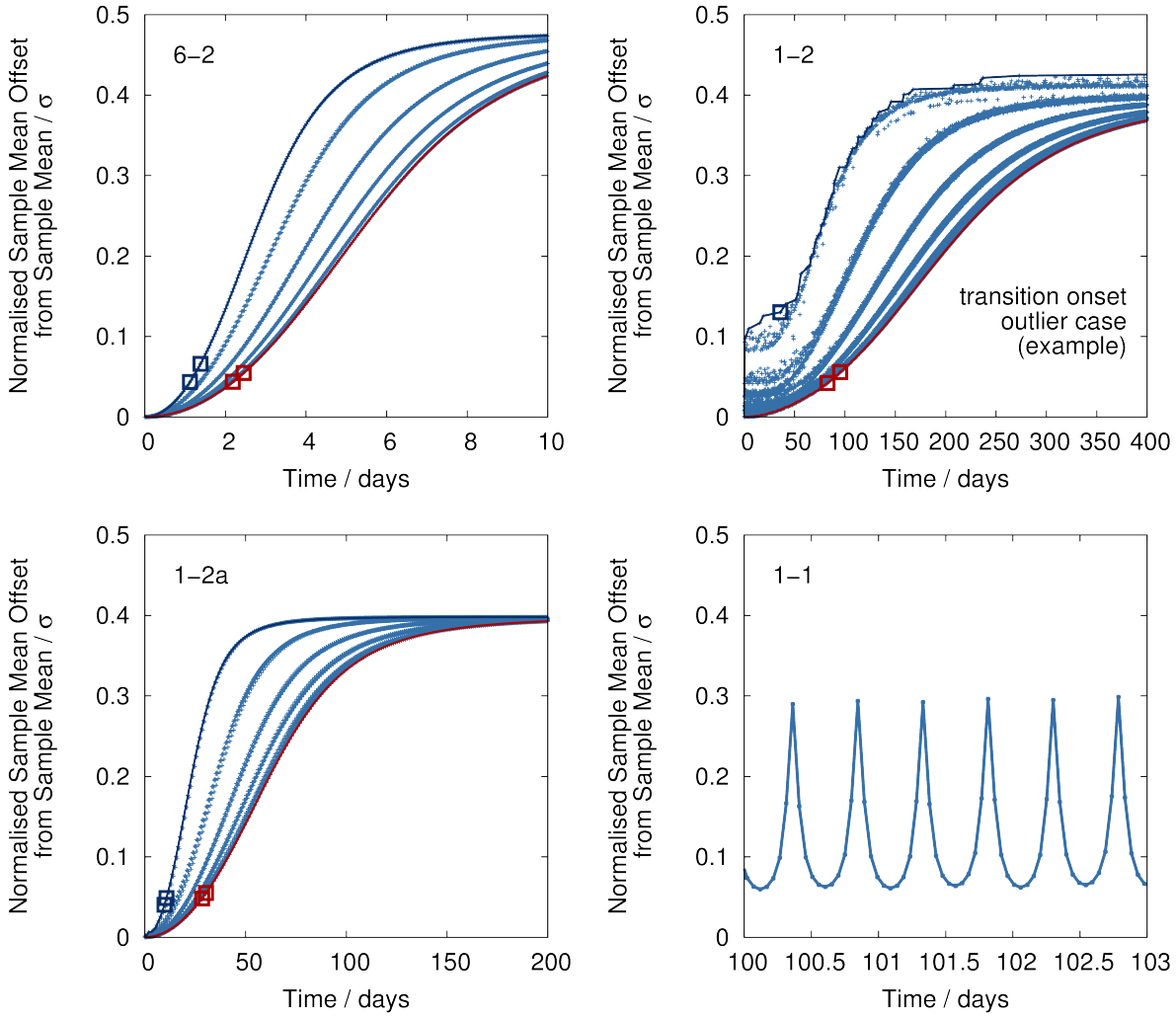

Figure 8: Example evolution of the normalised offset of the sample mean from the covariance mean. The image on the lower right is a close-up. It shows that the metric has the potential of indicating at each epoch the normality of the uncertainty.

4.2 MVN Validity Timeframe

Tab. 5 shows the MVN validity period based on the Henze-Zirkler test statistic using 25 Monte-Carlo runs. For the Transition Start phase, the Unscented Transform Based method outlined in Section 3.1 is used for comparison and further validation. Based on presented results, the method should be equally applicable to estimate the conclusion of the transition phase. MVN breakdown is flagged, when the sample mean drifts by more than 0.05 from the covariance mean in whitened space. This threshold is defined loosely based on the results from Section 3.1. The highest deviations between the two methods are observed for the cases with short time frames until onset of MVN breakdown. As breakdown initially occurs only once or twice an orbit, a difference of one orbit between methods has a higher relative deviation than for cases where the same difference is obtained but at a later breakdown onset epoch. Some of these deviations are due to the

variability of the Monte-Carlo results. It is not likely that the nature of the efficient method has a non-negligible contribution. These and other factors remain to be investigated.

Table 5: Beginning and end of transition into non-Gaussianity of position uncertainty using the *HZ* Test Statistics and 25 Monte-Carlo runs without variability of results based on CLT. For the transition onset, the unscented transform based method is applied using an MVN breakdown decision threshold of 0.05.

OD Id	**Transition starts**				**Transition ends**
	MVN_{HZ} [days]	MVN_{UT} [days]	Deviation [days]	[%]	Mean [days]
Geosynchronous Orbits					
3715	84.8	86.5	+1.7	+2.0	169.5
3721	142.6	129.4	-13.2	-9.3	239.4
3778	2.0	1.6	-0.4	-20.0	80.8
3783	within 1st orbit	0.5	0.0	0.0	235.4
Low Earth Orbits					
3769	31.4	25.7	-5.7	-18.2	70.1
3753	18.4	12.5	-5.9	-32.1	44.9
Medium Earth Orbits, Near Circular					
3739	92.4	96.5	4.1	+4.4	124.8
Medium Earth Orbits, Eccentric					
3073	87.4	79.9	-7.5	-8.6	479.5
3062	within 1st orbit	0.1	0.0	0.0	0.3

5 SUMMARY & OUTLOOK

The Henze-Zirkler test for Multivariate Normality is used to test random samples drawn from an initial covariance matrix and propagated through time using two-body motion. A structure is observed in the time evolution of this parameter when Monte-Carlo analysis is employed which seems to underlie samples drawn from any initial covariance matrix and in any orbit regime. After a period of remaining normally distributed over the entire orbit, the state uncertainty enters a phase of transition wherein it will become non-normally distributed for increasing parts throughout an orbit. Finally, the state uncertainty remains non-normally distributed throughout the entire orbit.
The method has been applied to state and covariances detailed in a Monte-Carlo study of probability of collision methods by Alfano in 2009 as a baseline. An attempt is made of calibrating the decision threshold of a more efficient method against the created baseline. The method relies on the sample mean of the unscented transform from the

covariance mean in whitened space. Preliminary results do not exclude the possibility a calibration factor may exist which will allow the method to be applied to all OD uniformly. Further investigation will be performed to better assess its potential and its limitations. Following this, it is planned to apply the method to SERC ODs using a full force model numerical propagator. It is the intention to store information on the MVN breakdown along with the OD results to benefit follow-on processes such as e.g. close encounter analyses or scheduling tasks.

6 ACKNOWLEDGEMENTS

The authors would like to acknowledge the support of the Cooperative Research Centre for Space Environment Management (SERC Limited) through the Australian Government's Cooperative Research Centre Programme. Additional thanks go out to Dr. Michael Lachut for his input and efforts.

References

[1] Alfano, S. *Satellite conjunction Monte Carlo analysis*. Adv. Astronaut. Sci., 134:2007–2024, 2009.

[2] Alfriend, K. T. and Park, I. *When Does the Uncertainty Become Non-Gaussian*. Adv. Maui Opt. Sp. Surveill. Technol. Conf., 2016.

[3] DeMars, K., Bishop, R. and Jah, M. *Entropy-Based Approach for Uncertainty Propagation of Nonlinear Dynamical Systems*. ... Guid. Control. Dyn., 36(4):1047–1057, 2013.

[4] Farrell, P. J., Salibian-Barrera, M. and Naczk, K. *On tests for multivariate normality and associated simulation studies*. J. Stat. Comput. Simul., 77(12):1065–1080, 2007.

[5] Flegel, S. K., Möckel, M. and Bennett, J. *Covariance Size and the Breakdown of Gaussianity in GEO Uncertainty Predictions*. Proceedings of the 7th European Space Debris Conference, 2017.

[6] Henze, N. and Zirkler, B. *A class of invariant consistent tests for multivariate normality*. Commun. Stat. - Theory Methods, 19(10):3595–3617, 1990.

[7] Julier, S. and Uhlmann, J. *Unscented Filtering and Non Linear Estimation*. Proc. IEEE, 92(3):401–422, 2004.

[8] Julier, S. J. and Uhlmann, J. K. *Correction to "Unscented Filtering and Nonliner Estimation"*. 2004.

[9] Mardia, K. *Measures of multivariate skewness and kurtosis with applications*. Biometrika, 57:519–530, 1970.

[10] Mecklin, C. J. and Mundfrom, D. J. *A Monte Carlo comparison of the Type I and Type II error rates of tests of multivariate normality*. J. Stat. Comput. Simul., 75(2):93–107, 2005.

[11] Oltrogge, D. L. *Efficient Solutions of Kepler's Equation via Hybrid and Digital Approaches*. AIAA/AAS Astrodyn. Spec. Conf. - AIAA, pages 401–420, 2014.

[12] Romeu, J., Oztur, A. *A comparative study of goodness-of-fit tests for multivariate normality*. Journal of Multivariate Analysis, 46:309–334, 1993.